Design of Torque Actuators Based on Ferromagnetic Shape Memory Alloy Composites

Minoru Taya*, Taishi Wada, Masahiro Kusaka and Ryan C.C. Lee
Center for Intelligent Materials and Systems, Univ. of Washington,
BOX 352600, Seattle, WA98195-2600, USA

Abstract

A new first generation torque actuator based on ferromagnetic shape memory alloy composite is designed. The first generation actuator made of Fe bars and TiNi wires is successfully demonstrated. A simple model is proposed for prediction of angle of twist for a given constant load. The optimization of FSMA composite plate is made by a composite modeling under the constraints that the super-elastic SMA plate attains higher stress beyond the onset of the stress-induced martensite transformation while the ferromagnetic plate remains elastic.

Keywords, ferromagnetic shape memory alloy, composite, torque actuators, super-elastic behavior

1. INTRODUCTION

Ferromagnetic shape memory alloys (FSMA) have attracted a strong attention among material science and actuator research community, as the speed of actuator based on FSMA is considered very fast, yet some of FSMA provide large stress. We proposed hybrid mechanism as the best way to design actuators with a capacity of large force and stroke [1,2], and designed spring actuators [3] and diaphragm actuators based on FSMA and FSMA composites[4]. The former provides large stroke and modest force while the latter for vibrating mode of the diaphragm thus, providing a jet flow. Among various actuators, torque actuators are very useful for a number of applications. Therefore we made some preliminary design of torque actuators based on FSMA composites. In this paper, we will report the preliminary results of the design of the torque actuators based on FSMA composite. First we discuss the design concept, followed by the design of first generation torque actuator. Then, we will discuss the modeling of a torque actuator made of plate spring, and also the modeling of composite plate bending which will be used as a key FSMA composite for torque actuators.

2. DESIGN CONCEPT AND FIRST GENERATION TORQUE ACTUATOR

We will discuss the difference of the mechanism between a conventional torque motor and the proposed torque actuator based on FSMA composite, then the design concept of the new torque actuator, followed by the statement of the first generation of the FSMA composite torque actuator. Figure 1(a) shows one example of a motor in which the rotor is electromagnet and the outer is permanent magnet. The rotor rotates owing to the power of the attraction and of the repulsion between the magnets. The relative motion between the electro and permanent magnets is a kind of sliding motion as shown in Fig.1 (b), where the North Pole of the permanent magnet is attracted to the South Pole of the electromagnet and moves along the x-axis due to the attractive force F_x between the magnets. On the other hand, the attractive force F_y, as shown in Fig.1(c), is not available for the rotating type of the conventional motors of Fig.1(a). It is because that in the configuration of Fig.1 (b) the permanent magnet can not move anymore once it is attracted to the electromagnet and comes into contact with it hence the preventing the rotating motion of a motor.

However, generally speaking, the force F_y is much larger than the force F_x, especially when the distance y between the magnets is small, although it depends on the gap between the magnets (See Fig.1(b) and (c)). The motor presented here moves rotationally by using the force F_y, and therefore the output torque expected to be powerful.

* corresponding author: tayam@u.washington.edu

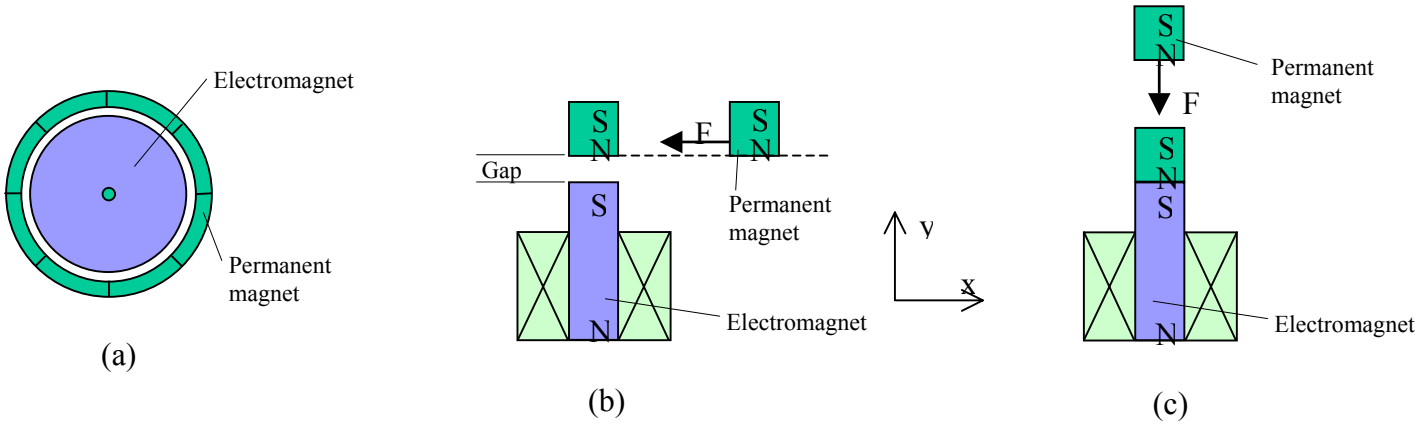

Fig.1. Relative motion between a permanent magnet and a electromagnet.

The design concept of a new torque actuator based on FSMA composite is illustrated in Fig. 2 where (a) and (b) denote the case of switch off and on of the electromagnet system, respectively. The new torque actuator consists of inner rod which will rotate clock-wise upon switching on of the electromagnet system and outer casing. The outer casing is composed of hybrid magnet made of permanent magnets and electromagnets, thus, attracting the FSMA plate spring to its inner wall upon switching on of the electromagnet system. The rotating motion of the inner rod will provide torque work for dead load that is connected to the rod by pulley or belt. The FSMA composite can be composed of ferromagnetic material and super-elastic grade shape memory alloy (SMA),and it is subjected to bending moment which is not uniform over the length of plate spring due to varying curvature. The requirements of the design of FMSA composite torque actuators, are (i) inducing the large stress so that the SMA plate in the composite plate can reach at least the onset of stress-induced martensite transformation, and the stress induced in the ferromagnetic plate remains still below its yield stress while the ferromagnetic plate should be attracted to the inner wall of the outer casing due to strong magnetic flux gradient upon switching on of the electromagnet system. The processing of FSMA composite plates itself is a formidable task, so we first designed a simple torque actuator based on ferromagnetic material (soft Fe bars) and TiNi wires of super-elastic grade SMA material to see if this would work. Figure 3 shows the first generation torque actuator where (a) and (b) denote the case of switch off and on, respectively. This torque actuator exhibited modest torque capability (0.588 N-m) and maximum angle of twist (45 degree).

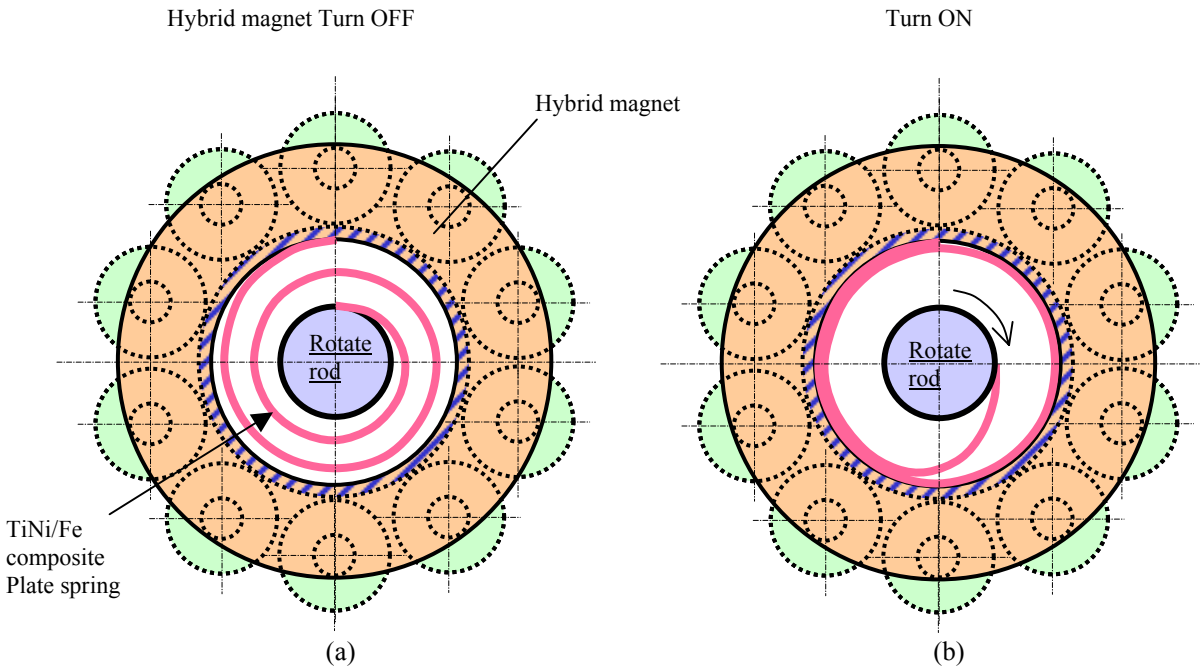

Fig 2. Concept of a new torque actuator based on FSMA composite, (a) switch off, (b) switch on of the electromagnet system.

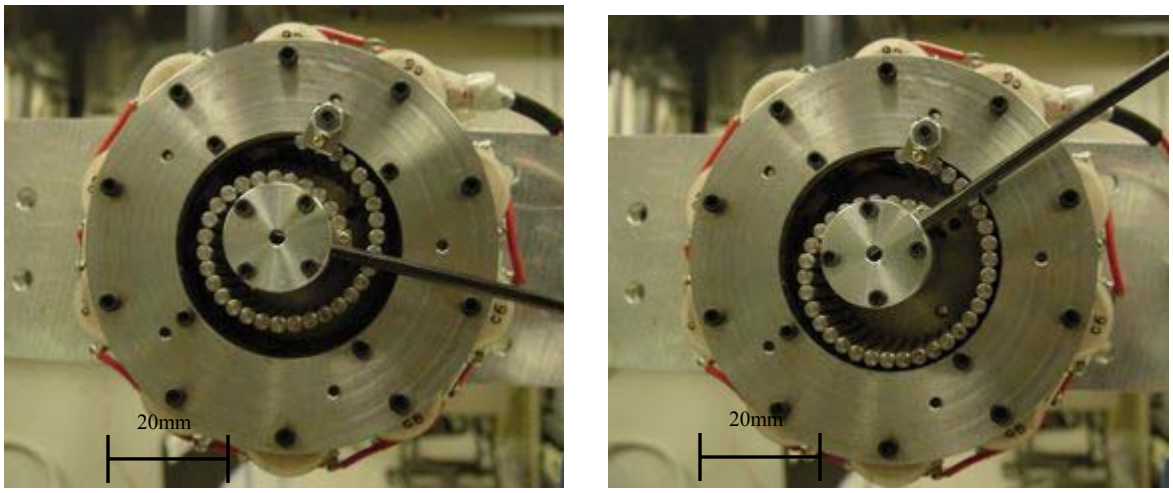

(a) (b)

Fig. 3 Photos of the first generation torque actuator made of Fe bars and TiNi wires, (a) switch off, (b) on of the electromagnet system.

3. MODELING OF TORQUE ACTUATOR

Consider a plate spring connected to the inner rod with radius r_0 at point P_0 and to the outer casing with innermost radius r_1 at point P_e where the rod is loaded with constant force, F_0, Fig. 4(a). Upon switching of the electromagnet system thus, a portion of the plate spring (arc P_e-P_2 in Fig. 4(b)) of length $\boldsymbol{l}$ is attracted to the inner wall, see Fig. 4(b), resulting in the rotation in counter-clockwise direction by angle ϕ, at this moment, the plate spring is bent around the inner rod with tangent point at P_1'. We examine the difference of strain energy between the initial (Fig. 4(a)) and current configuration (Fig. 4(b)), ΔE, which is equated to the work done by a constant force, F_o.

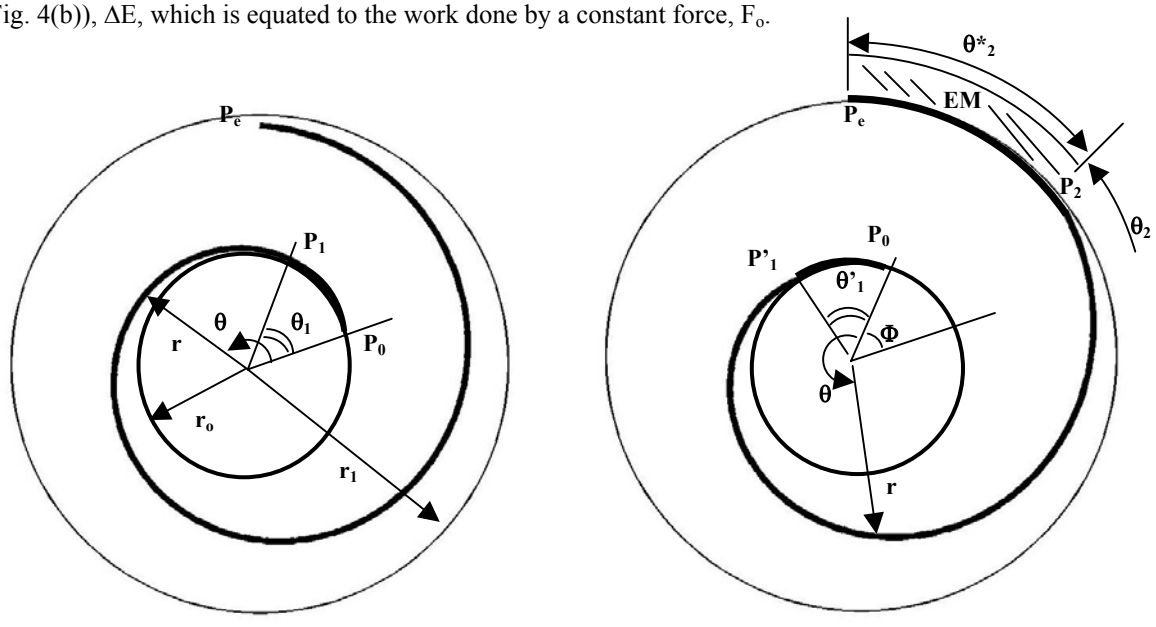

(a) (b)

Fig. 4 Model for torque actuator, (a) initial configuration and (b) current configuration when the electromagnet system is switched on, so that the plate spring of length l ($\overline{P_e P_2}$) is attracted to the wall.

Let the energy of Fig 4(a) and (b) are denoted as E_a and E_b, respectively. Then, we have an energy balance equation under a constant weight F_o,

$$\Delta E = E_a - E_b = F_0 l_0 \phi \tag{1}$$

where l_0 is the lever of the torque that can transmit a constant load F_o.

Referenced to Fig.4, when the power is not turned on, the radius r of each point in the plate spring is

$$r = \frac{(\theta - \theta_1)}{(2n\pi - \theta_1)}(r_1 - r_0) + r_0 \text{ , for } \theta_1 \le \theta \le 2n\pi \tag{2}$$

Then the free length of the spring, which is not attached to both the inner rod and the outer casing, is

$$L - r_0\theta_1 = \int_{\theta_1}^{2n\pi} r d\theta = \int_{\theta_1}^{2n\pi} \left[\frac{(\theta - \theta_1)}{(2n\pi - \theta_1)}(r_1 - r_0) + r_0 \right] d\theta = \frac{1}{2}(r_1 + r_0)(2n\pi - \theta_1) \tag{3}$$

From (2), θ_1 is solved as

$$\theta_1 = \frac{2[n\pi(r_0 + r_1) - L]}{(r_1 - r_0)} \tag{4}$$

The strain inside a elastic plate spring is $\varepsilon = \frac{y}{r}$, hence the stress is $\sigma = \frac{Ey}{r}$

So the elastic energy of the plate spring of Fig. 4(a), E_a is given by

$$E_a = \int_V (\frac{1}{2}\sigma\varepsilon) dV = \int_V \frac{Ey^2}{2r^2}(bdy)dl = \int_{\overline{P_0P_1}} \frac{Ey^2}{2r_0^2}(bdy)(r_0\theta_1) + \int_{\overline{P_1P_e}} \frac{Ey^2}{2r^2} bdy(rd\theta)$$

since $$\int_{\overline{P_0P_1}} \frac{Ey^2}{2r_0^2}(bdy)(r_0\theta_1) = \frac{r_0\theta_1 bE}{2r_0^2} \int_{-\frac{h}{2}}^{\frac{h}{2}} y^2 dy$$

and $$\int_{\overline{P_1P_e}} \frac{Ey^2}{2r^2} dy(rd\theta) = \frac{Eb}{2} \left[\int_{-\frac{h}{2}}^{\frac{h}{2}} \int_{\theta_1}^{2n\pi} \frac{y^2}{r^2} bdy(rd\theta) \right]$$

E_a is reduced to $E_a = \frac{bh^3 E\theta_1}{24r_0} + \frac{bh^3 E}{24} \int_{\theta_1}^{2n\pi} \frac{1}{r} d\theta$ (5)

In the above equations, b is the width of the plate spring.

With $r = \frac{(\theta - \theta_1)}{(2n\pi - \theta_1)}(r_1 - r_0) + r_0$, and performing integral, we obtain E_a as

$$\mathrm{E_a} = \frac{bh^3E}{24r_0}\left[\frac{2[n\pi(r_0+r_1)-L]}{(r_1-r_0)}+\frac{r_0}{(r_1-r_0)}\left(\ln(\frac{r_1}{r_0})\right)\left[\frac{2L-4n\pi r_0}{(r_1-r_0)}\right]\right] \tag{6}$$

Upon the switching on, the configuration of the torque actuator will become that of Fig. 4 (b).
The radius r of each point on the spring is given by

$$r = \frac{(\theta-\theta_1')}{(\theta_2-\theta_1')}(r_1-r_0)+r_0 \text{ , for } \theta_1' \le \theta \le \theta_2 \tag{7}$$

From the geometry of Fig. 4(b), $\theta_2 = 2n\pi - \theta_2^*$, where $r_1\theta_2^* = l$, therefore we have $\theta_2 = 2n\pi - \frac{l}{r_1}$ (8)

Then the free length of the spring, which is not attached to both the inner rod and the outer casing, is

$$L-l-r_0\theta_1' = \int_{\theta_1'}^{\theta_2} r\,d\theta \ , \tag{9}$$

with (7), (9) is reduced to

$$L-l-r_0\theta_1' = \int_{\theta_1'}^{\theta_2}\left[\frac{(\theta-\theta_1')}{(\theta_2-\theta_1')}(r_1-r_0)+r_0\right]d\theta = \frac{1}{2}(r_1+r_0)(\theta_2-\theta_1') \tag{10}$$

From (10), θ_1' is solved as

$$\theta_1' = \frac{2[n\pi(r_0+r_1)-L]}{(r_1-r_0)}+\frac{l}{r_1} \tag{11}$$

Let us evaluate the strain energy stored in the plate spring of Fig. 4, $\mathrm{E_b}$:

$$\begin{aligned}\mathrm{E_b} &= \int_V (\frac{1}{2}\sigma\varepsilon)dV = \int_V \frac{Ey^2}{2r^2}(bdy)dl \\ &= \int_{\overline{P_0P_1'}} \frac{Ey^2}{2r^2}(bdy)(rd\theta) + \int_{\overline{P_1'P_2}} \frac{Ey^2}{2r^2}bdy(rd\theta)\end{aligned} \tag{12}$$

since r is constant in the first and the third terms in (12),

$$\int_{\overline{P_0P_1'}} \frac{Ey^2}{2r^2}(bdy)(rd\theta) = \frac{bh^3E}{24r_0}\theta_1' \ , \tag{13}$$

We perform elemental integration for arc $\overline{P_1'P_2}$ by using (7) to obtain the second term,

$$\int_{\overline{P_1'P_2}} \frac{Ey^2}{2r^2}bdy(rd\theta) = \frac{bh^3E(\theta_2-\theta_1')}{24(r_1-r_0)}\ln(\frac{r_1}{r_0})$$

Therefore, E_b is obtained as

$$E_b = \frac{bh^3E}{24r_0}\left[\left[\frac{2[n\pi(r_0+r_1)-L]}{(r_1-r_0)}\right]+\frac{l}{r_1}+\frac{r_0}{(r_1-r_0)}\left(\ln\frac{r_1}{r_0}\right)\left[\frac{(2L-4n\pi r_0)}{(r_1-r_0)}-\frac{2l}{r_1}\right]\right] \tag{14}$$

From (1),(6) and (14), we have

$$E_a - E_b = F_0 l_0 \phi = \frac{bh^3E}{24r_0}\left[\frac{l}{r_1}-\frac{r_0}{(r_1-r_0)}\frac{2l}{r_1}\left(\ln\frac{r_1}{r_0}\right)\right] \tag{15}$$

From (15), we can calculate the angle of twist ϕ for a given constant load F_o as

$$\phi = \frac{bh^3E}{24r_0 l_0 F_0}\frac{l}{r_1}\left[1-\frac{2r_0}{(r_1-r_0)}\left(\ln\frac{r_1}{r_0}\right)\right] \tag{16}$$

We made a parametric study based on the above model, using eq (16) where the effects of size of the actuator on the torque angle (ϕ) are examined, i.e thickness (h) and width of the plate spring (b), number of turns of the plate spring (n), load ($F_{o)}$. Fig. 5 denotes the predicted results of plate width (b) for several cases of plate thickness (h). It indicates positive influence of the thickness of the plate on the increasing of ϕ. The width of the plate also contributes positively for the load carrying capability of the actuator. This is reasonable since the bigger the plate spring, the more energy can be stored in the spring as strain energy. Upon actuation of the electromagnets, more energy can be released from the plate spring.

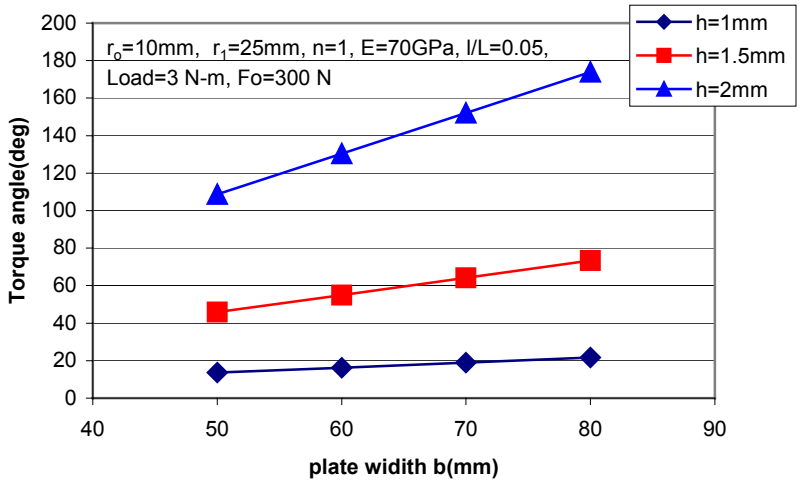

Fig. 5torque angle vs. width of plate spring predicted by the present model where $r_0 = l_0$ was used.

A comparison between the preliminary experiment and prediction by the model

Since the plate spring used in our experiment is made of Fe bars and two TiNi wires, we have to convert this to equivalent plate spring with rectangular cross section. Assuming that only two TiNi wires support the bending stress, we estimated that the width (b) and height (h) of the equivalent plate spring are,
b=3 mm, h=1.5 mm.
The parameters are used and measured in the experiment are,
r_0=10mm, r_1=25mm, l_0=80 mm, F_0=7.35 N, l =59mm, ϕ=58 degree,

torque = $F_0 l_0$ =0.588 N-m. (17)

The range of radius of curvature (r) is calculated from ρ = r_0 to r_1, thus the range of the maximum bending strain ($\varepsilon = y_{max} / r$) with y_{max} =0.75 mm, ε = 0.03 ~ 0.07. This range of the strain in TiNi wires correspond to the superelastic plateau of the stress-strain curve of TiNi. This would support the assumption that TiNi wires undergo stress-induced martensite transformation, i.e, superelastic plateau. Then the range of the maximum bending stress can be estimated by the range of ε multiply by Young's modulus ($E_A \sim E_m$) where E_A and E_m are the Young's modulus of 100% austenite and 100% martensite phase, respectively and they are given by

E_A= 80 GPa, E_m= 50 GPa. (18)

If the parameters in Eq.(17) and (18) are used to calculate torque angle, ϕ by Eq(16), we obtain the range of torque angle

ϕ =90 ~ 144 degree. (19)

The value of ϕ so estimated , Eq(19), overestimates the measured value of 58 degree, but the order of the estimated ϕ is in the same order as that of the experiment.

4. MODELING OF FSMA COMPOSITE PLATES

The deformation mode of the plate spring discussed in the previous section is bending, and the plate is composite composed of ferromagnetic plate and super-elastic grade SMA plate, it is assumed here that the FSMA composite plate is subjected to a pure bending moment, M to facilitate the modeling although the actual plate spring is loaded with varying bending moment due to varying curvature. The modeling of the FSMA composite plate under pure bending is illustrated in Fig 6 where (a) and (b) denote the schematic of bent FSMA composite plate of thickness h under M, resulting in curvature ρ the stress-strain curves of super-elastic SMA and ferromagnet material (only loading up to the yield stress is shown in Fig.6), respectively. It is noted in Fig.5 (6) that the ferromagnetic plate with thickness h_f, is bent convex toward the inner wall of the outer casing, so that it can be attracted to the electromagnetic system upon switching on. The requirements of the FSMA composite design are such that the bending stress in ferromagnetic plate remain elastic just below the yield stress while that in the SMA plate can be reached to the plateau of the stress-induced martensite phase transformation, i.e., super-elastic region. It is assumed in the present model that the super-elastic region is flat rectangular box, ignoring work-hardening rate, see Fig. 7 (a). The stress distribution in FSMA composite can be classified into the following three cases:

Case-1: the bending stress in ferromagnetic plate just reaches the yield stress while that of the SMA plate is below the onset (σ_{SIM}) of stress-induced martensite (SIM).

Case-2: the bending stress in ferromagnetic plate just reaches the yield stress while that in the SMA plate is already on the super-elastic plateau., σ_{SIM}

Case-3: the bending stress in ferromagnetic plate just reaches the yield stress while in all the SMA plate the stress is above the onset of SIM stress level, σ_{SIM}

For constituent SMA material, we consider CuMnAl material that has been investigated by Tohoku University Group[5,6], as the super-elastic stress strain curve can be tailored to some extent by appropriate heat treatment with the level of σ_{SIM} being in the range of 180-250 MPa. For ferromagnetic material, we considered soft Fe and FeCoV plates. The yield stress of the former is around 200 MPa and that of the latter is 400 MPa. Preliminary results of the present modeling of the FSMA composite plate are shown in Fig. 7 where (a) and (b) denote, the stress-strain curves of the constituent materials, FeCoV as a ferromagnetic material and CuMnAl as a SMA with super-elastic behavior which is idealized as flat-rectangular shape for loop portion and non-work-hardening rate. Fig. 7(b) indicates clearly the superelastic bending behavior that can be realized by using the FMSA composite made of FeCoV and CuMnAl. Even if we predicted one of the optimum design of FSMA composite plate for the proposed torque actuators, the processing of such FSMA composite plates faces a formidable challenge.

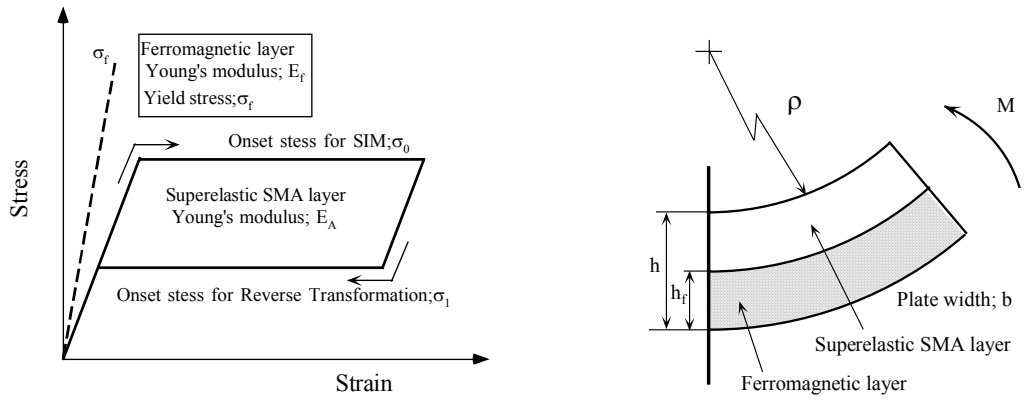

(a) Stress-strain relations for Fe and CuAlMn (b) Plate bending model

Fig.6 Material properties and model for the theoretical examination.

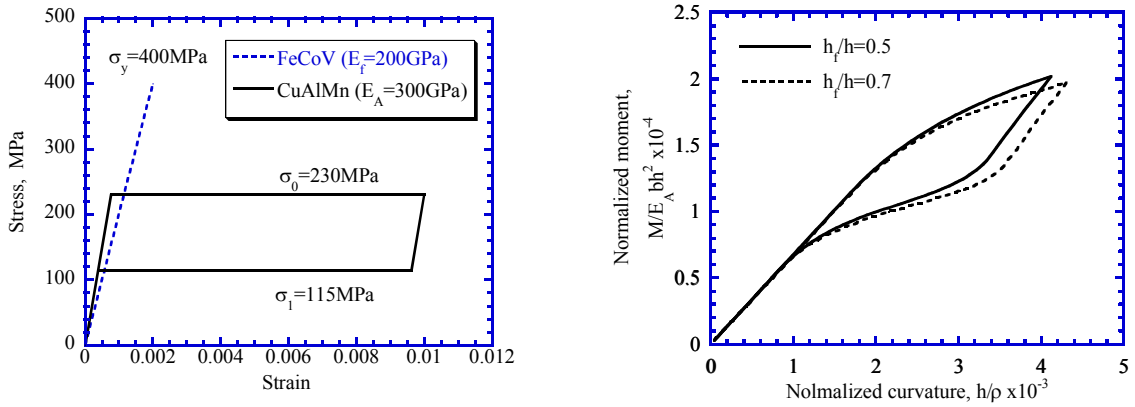

(a) (b)

Fig. 7 FSMA composite design for plate spring of the torque actuator, (a) stress-strain curves of FeCoV and CuMnAl, and (b) predicted bending moment-curvature relation of the composite plate under pure bending.

5. CONCLUSION

We proposed a new torque actuator based on FSMA composite, showing the first generation torque actuator that is assembled and successfully demonstrated. We constructed a simple model that can predict the level of angle of twist for a given constant dead load. Then, to make optimum design of the FSMA composite plate, we proposed a model by which the optimum design of FeCoV/CuMnAl composite is designed.

ACKNOWLEDGMENTS

The present study was supported by the contract (N-00014-00-1-0520) from Darpa/ONR on Design of Compact Actuator Program (CHAP) where Dr. John Main of Darpa and Dr. Roshdy Barsoum of ONR are the program monitors. This work is in part (composite modeling) is supported by a grant from AFOSR (F49620-02-1-0028) where Dr. Les Lee is the program manager. The author would also like to thank Dr. Y. Liang for his suggestions in refining the model.

References

1. H.Kato, T. Wada, T. Tagawa, Y. Liang and M. Taya, Proc. Of Mater. Sci. for the 21th Centrury, The Soc of Mater Sci of Japan, Vol. A. pp. 296-305, 2001.
2. H.Kato, T. Wada, Y. Liang, T. Tagawa, M. Taya and T. Mori, Mater Sci. Eng. Vol.A332, pp. 134-139, 2002.
3. T. Wada and M. Taya, Proc of SPIE on Smart Structures and Materials, ed C. S. Lynch,, vol.4699, pp. 294-302, 2002
4. Y. Matsunaga, T. Tagawa, T. Wada and M. Taya, Proc. SPIE on Smart Structures and Materials, ed C. S. Lynch, vol. 4699, pp.172-181.

5. Y. Sutou, R. Kainuma and K. Ishida, Mater. Sci. Eng. A, 273-275, pp.375-379, 1999.
6. Y. Sutou, T. Omori, R. Kainuma, N. Ono and K. Ishida, Metal. Mater. Trans. A, 33A, pp2817-2824, 2002.